

# Pole trajectories of the $\Lambda(1405)$ help establish its dynamical nature

Zejian Zhuang,<sup>1,\*</sup> R. Molina,<sup>1,†</sup> Jun-Xu Lu,<sup>2,‡</sup> and Li-Sheng Geng<sup>2,3,4,5,§</sup>

<sup>1</sup>*Departamento de Física Teórica and IFIC, Centro Mixto Universidad de Valencia-CSIC, Parc Científic UV, C/ Catedrático José Beltrán, 2, 46980 Paterna, Spain*

<sup>2</sup>*School of Physics, Beihang University, Beijing 102206, China*

<sup>3</sup>*Beijing Key Laboratory of Advanced Nuclear Materials and Physics, Beihang University, Beijing 102206, China*

<sup>4</sup>*Peng Huanwu Collaborative Center for Research and Education, Beihang University, Beijing 100191, China*

<sup>5</sup>*Southern Center for Nuclear-Science Theory (SCNT), Institute of Modern Physics, Chinese Academy of Sciences, Huizhou 516000, China*

Chiral trajectories of dynamically generated resonances are intimately connected to the SU(3) breaking pattern and their nature. From an analysis of a recent LQCD simulation on the  $\pi\Sigma - \bar{K}N$  scattering for  $I = 0$  and the study of the quark mass dependence of the octet baryon masses, we determine for the first time unambiguously the trajectories of the two poles associated to the  $\Lambda(1405)$  towards the symmetric point over the  $\text{Tr}[M] = C$  trajectory accurately. At  $m_\pi \simeq 200$  MeV, our results are consistent with the lattice simulations, and the extrapolations to the physical point, based on the NLO chiral Lagrangians, agree well with existing experimental analyses. We predict qualitatively similar trajectories at LO and up to NLO, consistent with the LO interaction's dominance. At the SU(3) symmetric point up to NLO in this trajectory, the lower pole is located at  $E^{(1)} = 1583(5)(1)$  MeV, being dominantly a SU(3) singlet, while the higher pole belongs to the octet representation with a mass of  $E^{(8)} = 1585(8)(2)$  MeV. We also make predictions on the evolution of the two poles over the  $m_s = m_{s,\text{phy}}$  trajectory. This can be tested in future LQCD simulations and experimental measurements.

## I. INTRODUCTION

The  $\Lambda(1405)$ , discovered in bubble chamber experiments at low-energy  $K^-p$  scattering as a resonance decaying into  $\pi^-\Sigma^+$  [1, 2], has been a subject of controversy for a long time. This can be mainly attributed to the two-pole structure predicted in the chiral unitary approach, which refers to a lower pole above the  $\pi\Sigma$  threshold and a higher pole below the  $\bar{K}N$  threshold [3–15]. Only recently, the lower pole associated to the two-pole structure demanded by chiral dynamics and SU(3) flavor symmetry has been included in the PDG [16] about 60 years later.

Its quantum numbers are  $J^P = \frac{1}{2}^-$  [17]. Surprisingly, being the first negative parity excitation of the  $\Lambda$ , it is lighter than its nucleon counterpart by around 100 MeV. This can be naturally explained in the chiral unitary approach, considering the  $N^*(1535)$  and the  $\Lambda(1405)$  as dynamically generated resonances from the  $K\Lambda$ ,  $K\Sigma$  channels, and the  $\bar{K}N$ ,  $\pi\Sigma$  channels respectively, see [3, 5, 15, 18–20]. The interaction in these approaches is driven by the lowest order (LO) interaction in  $s$ -wave. This Weinberg-Tomozawa term is attractive and leads to two poles in the unphysical sheet. At NLO the two-pole structure also persists [13, 14, 21–25]. Some of the NLO low-energy constants (LECs) in the chiral lagrangian are constrained by the splitting of the baryon masses, the pion-nucleon sigma term, and the strangeness content of the proton [26]. Yet, because of the unitarization process, these are usually kept as free parameters adjusted to experimental data. On the other hand, there are experimental data from LEPS, CLAS, COSY, HADES [17, 27–31], which have been used to fix these NLO

parameters in theoretical analyses [32–34]. As a result of these analyses, the position of the higher pole is well constrained, while the position of the lower one is not. Recent NNLO studies have further supported the two-pole structure [35]. Both pole positions are determined more precisely by including the experimental data on  $\bar{K}N$ ,  $KN$ , and  $\pi N$  cross sections. This analysis yields,  $E_1 = [1392 \pm 8 - i(102 \pm 15)]$  MeV, and,  $E_2 = [1425 \pm 1 - i(13 \pm 4)]$  MeV. In all the studies based on the chiral unitary approach, the first pole couples more strongly to  $\pi\Sigma$ , while the second one, also seen in  $\pi\Sigma$ , couples more to  $\bar{K}N$ . For recent reviews of the  $\Lambda(1405)$ , see [36, 37]. The  $K^-p$  interaction and the presence of the two-pole structure have also been inferred from the measured femtoscopic correlation functions [15, 38, 39]. However, there is still controversy since the recent J-PARC line-shape data seem only to require the presence of one resonance [40].

In the past, the scarce lattice QCD (LQCD) simulations investigating the  $\Lambda(1405)$  have only considered single baryon three quark interpolating fields [41–49]. The difficulties in extracting the two poles from the LQCD data were emphasized in [50]. However, a recent LQCD simulation included the meson-baryon operators. These results were most welcome since, for the first time, a signature of the lower pole of the  $\Lambda(1405)$  has been observed as a virtual bound state at a pion mass of  $\sim 200$  MeV [51, 52]. The pole positions obtained in this simulation [51, 52] are,  $E_1 = 1392(9)(2)(16)$  MeV, and  $E_2 = 1455(13)(2)(17) - i 11.5(4.4)(4)(0.1)$  MeV. The lower pole couples more to  $\pi\Sigma$  with approximately double strength than to  $\bar{K}N$ , and the higher to  $\bar{K}N$ , with ratios of the couplings in line with earlier results based on the chiral unitary approach.

Nonetheless, in [51, 52], the parameterization used to extract the poles is based on the effective range expansion (ERE) and the  $K$ -matrix formalism, neglecting the real part of the loop function [3, 5]. In addition, a chiral extrapolation to the physical point from the analyses of the energy levels of [51, 52] to investigate the compatibility of the result with the

\* zejian.zhuang@uv.es

† raquel.molina@ific.uv.es

‡ ljxwohool@buaa.edu.cn

§ lisheng.geng@buaa.edu.cn

experimental data has not yet been done. The trajectories of the poles along the  $\text{Tr}[M] = C$  curve towards the SU(3) symmetric limit have not been studied either from the analyses of the energy levels obtained in LQCD.<sup>1</sup> We stress that these trajectories are a fundamental property of the  $\Lambda(1405)$  connected to the SU(3) breaking pattern and its nature as a dynamically generated resonance.

The first explorations of the trajectories of the  $\Lambda(1405)$  with increasing pion masses can be found in [53–57]. In [53, 54], where the earlier LQCD simulations were compared with the predictions of the chiral unitary approach, concluding that it was important to include meson-baryon interpolating fields in future simulations. In [55] the pole trajectories from the SU(3) limit to the physical values are investigated using the chiral unitary approach at NLO with LECs fixed to the experimental data on  $K^-p$  scattering [36]. The LECs used in this work,  $m_0$ ,  $b_i$ ,  $L_i$  contributing to the baryon, pseudoscalar meson masses, and decay constants at NLO, are based on previous analyses of scarce data for LQCD simulations that do not account for  $\pi\Sigma$  operators along the  $m_s = m_{s,\text{phy}}$  trajectory [49].

In [56], the pole trajectories in the LO chiral unitary approach are studied following the PACS-CS trajectory (for  $m_s = m_{s,\text{phy}}$ , within a range of pion masses from 137 to 497 MeV [58, 59]). In [57], the  $\Lambda(1405)$  pole trajectories for the CLS ensembles at leading order are studied in a renormalizable covariant chiral effective field theory formulation.

However, in none of the previous works [55–57], neither the energy levels for the  $\bar{K}N$  and  $\pi\Sigma$  scattering [51, 52] nor the most recent LQCD data of baryon masses [60] for the CLS ensembles have been analyzed. This step is essential to understand the SU(3) symmetry pattern of the  $\Lambda(1405)$  two poles, their nature, and the LQCD and experimental data consistency. In this work, we fill this gap by conducting the first extrapolation to the physical point from the analysis of the energy levels of [51, 52] and study the trajectories of the two poles towards the SU(3) symmetric line along the  $\text{Tr}[M] = C$  curve. This is a crucial test for the chiral unitary approach in future LQCD simulations and the two-pole structure of the  $\Lambda(1405)$ . Our work is based on the one-loop NLO covariant baryon chiral perturbation theory. We will also study the effect of the NLO terms on these trajectories with respect to the LO prediction. Moreover, we predict the evolution of the two-poles not only in the  $\text{Tr}[M] = C$  line, but also in the  $m_s = m_{s,\text{phy}}$  trajectory, and show that these are indeed very different due to the dynamical nature of the  $\Lambda(1405)$ .

## II. FORMALISM

The SU(3) chiral Lagrangians for the meson-baryon interaction are given in [61–64]. For *isospin*, *strangeness*,  $I = 0$ ,  $S = -1$ , we consider the four channels  $i, j = \pi\Sigma, \bar{K}N, \eta\Lambda, K\Sigma$ . The

interaction kernel up to NLO reads [12],

$$V_{ij} = -\frac{N_i N_j}{4f^2} [C_{ij}(2\sqrt{s} - M_i - M_j) - 4(D_{ij} - 2k_\mu k'^\mu L_{ij})] \quad (1)$$

where  $N_i = \sqrt{(M_i + E_i)/2M_i}$ , and  $M_i, E_i$  stand for the baryon mass and energy of channel  $i$ , respectively. The first term in Eq. (1) represents the Weinberg-Tomowawa (WT) interaction (LO), while the second one comes from the NLO lagrangian. In Eq. (1), the  $D_{ij}$  and  $L_{ij}$  coefficients are a combination of the pertinent LECs of  $b_0, b_D, b_F$ , and  $d_i, i = 1, 4$ . The LECs  $b_i$  and  $d_i$  stem from the NLO contact terms of the chiral lagrangians for the meson-baryon interaction [65, 66]. The LECs  $b_i$  are related to the splitting of the octet baryon masses and pion-nucleon sigma term [26] since they come from the Lagrangian terms proportional to the quark mass, and the LECs  $d_i$  appear only in the  $P_i B_j \rightarrow P_k B_l$  scattering ( $P =$  pseudoscalar meson,  $B =$  baryon). They contribute to the non-relativistic limit of the  $s$ -wave interaction. These combinations are given in Appendix A of [12]. See also [6]. We consider the one-loop covariant baryon chiral perturbation theory for the latter. The LECs  $b_i$  are fitted to the recent RQCD simulations on the quark mass dependence of baryon masses for the CLS ensembles [60], which include data on the  $m_s = m_{s,\text{phy}}$ ,  $\text{Tr}[M] = C$  and  $m_{u(d)} = m_s$  trajectories. The fit in this work is discussed in more detail in the Supplemental Material [67]. Table I gives the values obtained for these LECs- $b_i$ . The baryon mass obtained in the chiral limit is  $m_0 = 805(40)(40)$  MeV.

On the other hand, the masses of the pseudoscalar mesons are calculated up to NLO in ChPT. The quark mass dependence of the pseudoscalar meson masses  $m_\phi$  and decay constants  $f_\phi$ , with  $\phi = \pi, K, \eta$ , were investigated in [68] by analyzing the recent LQCD data including the CLS ensembles. In the present work, we use the NLO ChPT pseudoscalar masses and take the values of the LECs  $L$ 's obtained from the global fit, see Table X of [68]. Since both light and strange mesons are present in the channels  $i, i = 1, 4$ , we take the average  $f = (f_\pi + f_K + f_\eta)/3$  in Eq. (1). Therefore, the pion mass dependence on the decay constants is incorporated in our framework, taking into account recent LQCD data.

TABLE I. Values of the LECs- $b_i$  in units of  $\text{GeV}^{-1}$ . The first uncertainty is statistical and the second originates from the lattice spacing [60].

	$b_0$	$b_D$	$b_F$
This work	-0.665(40)(28)	0.062(26)(8)	-0.354(18)(9)
BChPT FV [60]	-0.739 <sup>(70)</sup> <sub>(84)</sub>	0.056 <sup>(43)</sup> <sub>(39)</sub>	-0.44 <sup>(40)</sup> <sub>(26)</sub>

The scattering amplitude in the infinite volume can be written as

$$T^{-1} = V_0^{-1} - G, \quad (2)$$

where  $V_0 \equiv V_{(L=0)}$  is the  $s$ -wave projection of Eq. (1), and  $G$  is a diagonal matrix with the meson-baryon loop functions,

<sup>1</sup> Here,  $M$  stands for the quark mass matrix, and the trajectory  $\text{Tr}[M] = C$  means  $m_u + m_d + m_s = C$ .

whose elements are

$$G_j = 2iM_j \int \frac{d^4q}{(2\pi)^4} \frac{1}{q^2 - m_j^2 + i\epsilon} \frac{1}{(P - q)^2 - M_j^2 + i\epsilon}. \quad (3)$$

The above equation can be evaluated using the dimensional regularization (DR) method or a cutoff  $q_{\max}$  [69]. Comparing the expressions obtained in the two schemes, one can obtain the dependence of the subtraction constant on the masses of the mesons and baryons in the loop. Here, we follow the relation obtained in Ref. [70], where,

$$a(\mu) = -\frac{2}{m_j + M_j} \left[ m_j \log \left( 1 + \sqrt{1 + \frac{m_j^2}{q_{\max}^2}} \right) + M_j \log \left( 1 + \sqrt{1 + \frac{M_j^2}{q_{\max}^2}} \right) \right] + 2 \log \left( \frac{\mu}{q_{\max}} \right). \quad (4)$$

and we set the scale  $\mu = 630$  MeV [3].

On the other hand, in the finite volume, neglecting the effects from higher partial waves, the scattering amplitude reads,

$$\tilde{T}^{-1} = V_0^{-1} - \tilde{G}. \quad (5)$$

The finite-volume loop function  $\tilde{G}$  can be calculated in the DR scheme as [71],

$$\tilde{G}(P^0, \vec{P}) = G^{DR}(P^0, \vec{P}) + \lim_{q_{\max} \rightarrow \infty} \Delta G(P_0, \vec{P}, q_{\max}), \quad (6)$$

being  $\Delta G = \tilde{G}^{co} - G^{co}$ ,  $G^{DR}$ , and  $G^{co}$ , the loop function in the infinite volume evaluated in the dimensional regularization (DR) and cutoff scheme (co), respectively [53]. In moving frames,  $\tilde{G}^{co}$  reads [72]<sup>2</sup>,

$$\tilde{G}^{co} = \frac{2M}{L^3} \sum_{\vec{n}} \frac{E}{P_0} I(|\vec{q}^*(\vec{q})|), \quad (7)$$

In the above equation,  $q^*$  is the center-of-mass (CM) frame momentum,  $\vec{q}_1^* + \vec{q}_2^* = 0$ , which can be written in terms of the momenta  $\vec{q} = 2\pi \frac{\vec{n}}{L}$  in the boosted frame with momenta  $P^\mu = q_1^\mu + q_2^\mu$ , and the squared energy in the CM frame is given by  $s = P_0^2 - \vec{P}^2$ . The function  $I(q)$  reads,

$$I(\vec{q}) = \frac{\omega_1(q) + \omega_2(q)}{2\omega_1(q)\omega_2(q) [P_0^2 - (\omega_1(q) + \omega_2(q))^2 + i\epsilon]}, \quad (8)$$

with  $\omega_i = \sqrt{q^2 + m_i^2}$ ,  $i = 1, 2$  refer to the meson ( $m_1 = m$ ) and baryon ( $m_2 = M$ ) in the loop, and  $q = |\vec{q}|$ . Neglecting the effects from higher partial waves, the energy levels are given solely by [72],

$$\det [I - V_0 \tilde{G}] = 0. \quad (9)$$

Near the resonance region around  $\sqrt{s_0}$ , the coupling  $g_i$  to the  $i$ th meson-baryon channel can be easily evaluated since the amplitude behaves as

$$T_{ij} \simeq \frac{g_i g_j}{\sqrt{s} - \sqrt{s_0}}. \quad (10)$$

Once the interaction  $V_0$  is obtained from a fit to the energy levels through Eq. (9), phase shifts can be readily obtained through Eq. (2),

$$p \cot \delta_j = -\frac{8\pi E}{2M_j} (T_{jj})^{-1} + i p_j. \quad (11)$$

### III. RESULTS AND DISCUSSIONS

We analyze the energy levels of Refs. [51, 52] for  $m_\pi \simeq 200$  MeV through Eq. (9), with the  $s$ -wave projection of the NLO interaction given by Eq. (1). The  $\chi^2$  is given by

$$\chi^2 = \Delta E^T C_E^{-1} \Delta E, \quad (12)$$

where  $C_E$  is the covariance matrix for the energy levels, which is evaluated from the raw data of Ref. [51], and  $\Delta E_i = E_i' - E_i$  is the difference between the lattice energy level  $E_i$  and the predicted one  $E_i'$ . The resulting energy levels for the two-coupled-channel finite volume scattering are given in Fig. 1. The LQCD energy levels are very well reproduced by the interaction up to NLO. We have included the first four energy levels in the fit, with all data points shown in Fig. 1. The LECs- $b_i$  are determined by reproducing the quark mass dependence of the baryon masses along the trajectories of the CLS ensembles [60], and the  $d_i$  are fitted to the energy levels. The value of the reduced- $\chi^2$  obtained is  $\chi_{\text{dof}}^2 = 2.3$ . If the correlation matrix between the energy levels is omitted, the value obtained is  $\chi_{\text{dof}}^2 = 0.5$ . Thus, the correlation matrix significantly constrains the NLO LECs. The results of the LECs  $d_i$  are given in Table II. The cutoff  $q'_{\max}$  in Eq. (4) obtained in this fit is 710(39)(40) MeV.

TABLE II. Results for the LECs  $d_i$  in units of  $\text{GeV}^{-1}$ . The second error comes from the uncertainty in the lattice spacing [51, 52].

$d_1$	$d_2$	$d_3$	$d_4$
-0.36(20)(20)	0.02(1)(1)	-0.14(10)(10)	-0.58(20)(20)

In Fig. 2, we show the pole positions at the 1- $\sigma$  confident level (68%), where the colors denote the strength of the couplings  $|g_i|$ . We find two poles, the lower pole being mostly a virtual state, whereas the higher pole corresponds to a resonance below the  $\bar{K}N$  threshold.

The SU(3) limit over the  $\text{Tr}[M] = C$  curve is reached at  $m_\pi = 423$  MeV with a baryon mass  $m_B = 1182(7)(5)$ . In Table III, we give the positions and couplings of the poles for  $m_\pi = 138, 200, \text{ and } 423$  MeV. The positions

<sup>2</sup> Note that Lorentz symmetry is broken in the finite volume.

of the two poles agree very well with the values obtained in LQCD, which are  $z_1 = 1392(9)(2)(16)$  MeV and  $z_2 = 1455(13)(2)(17) - i11.5(4.4)(4)(0.1)$  for  $m_\pi \approx 200$  MeV. The ratios of the couplings obtained in the LQCD simulation are [51, 52],

$$\left| \frac{g_{\pi\Sigma}^{(1)}}{g_{\bar{K}N}^{(1)}} \right| = 1.9(4)_{\text{st}}(6)_{\text{md}}, \quad \left| \frac{g_{\pi\Sigma}^{(2)}}{g_{\bar{K}N}^{(2)}} \right| = 0.53(9)_{\text{st}}(10)_{\text{md}}, \quad (13)$$

where the first ratio is for the lower pole and the second one is for the higher pole, also agree very well with the values that we obtain; see the third and fourth row of Table III. Note that while the first pole couples strongly to  $\pi\Sigma$ , the second one does to  $\bar{K}N$  with the above ratios being compatible with the LQCD study [51, 52]. When the extrapolation to the physical point of the two-coupled-channel calculation is performed, the position of the higher pole at  $m_\pi = 138$  MeV also agrees remarkably well with previous experimental data analysis, as shown in Fig. 3. Furthermore, we can compare our results with the available experimental cross-sections of Ref. [36]. Remarkably, without conducting a fit to these data, our results agree well with the experimental cross-sections. See Fig. 4. Hence, an agreement between the LQCD, experimental data, and the chiral unitary approach is found for the first time. This strongly supports the quark mass dependence obtained here, which is determined reliably and includes all sources of quark mass dependence. Notice that in previous works, only qualitative results were obtained [5, 55–57, 73]. For  $m_\pi \approx 200$  MeV, we also obtain phase shifts that resemble the ones obtained in Refs. [51, 52] as shown in the Supplemental Material [67].

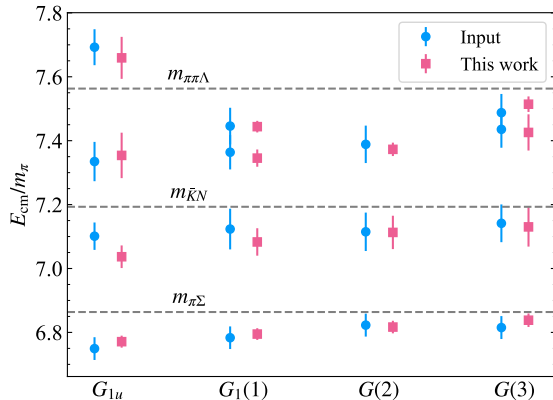


FIG. 1. Finite-volume spectrum in the center-of-mass frame used as inputs to constrain the LECs of the chiral Lagrangian up to NLO.

Next, we comment on the results obtained in the SU(3) limit, which is based on a four-coupled-channel calculation, including  $\eta\Lambda$  and  $K\Xi$ , as predictions from the two-coupled-channel LQCD analysis. At LO, the two higher poles become degenerate, and we obtain  $E^{(1)} = 1549(7)$  MeV,  $E^{(8)} = E^{(8')} = 1602(4)$  MeV. Up to NLO, we obtain three poles in the physical sheet with energies,  $E^{(1)} = 1583(5)(1)$  MeV,

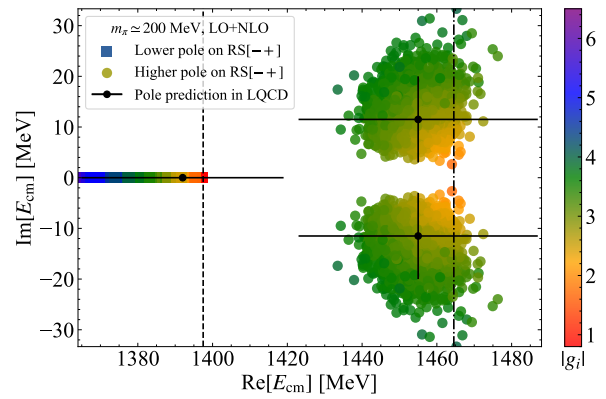


FIG. 2. Pole positions of the  $\Lambda(1405)$  for  $m_\pi \approx 200$  MeV at  $1\text{-}\sigma(68\%)$  confidence level. The error bars in black denote the LQCD results. The dashed line represents the  $\pi\Sigma$  threshold, and the dot-dashed line is the  $\bar{K}N$  threshold.

$E^{(8)} = 1585(8)(2)$  MeV, and  $E^{(8')} = 1601(12)(2)$  MeV.<sup>3</sup> We obtain a small breaking at NLO, i.e.,  $\Delta E = E^{(8')} - E^{(8)} = 16$  MeV, and both  $\Lambda(1405)$  poles are located on the physical sheet.

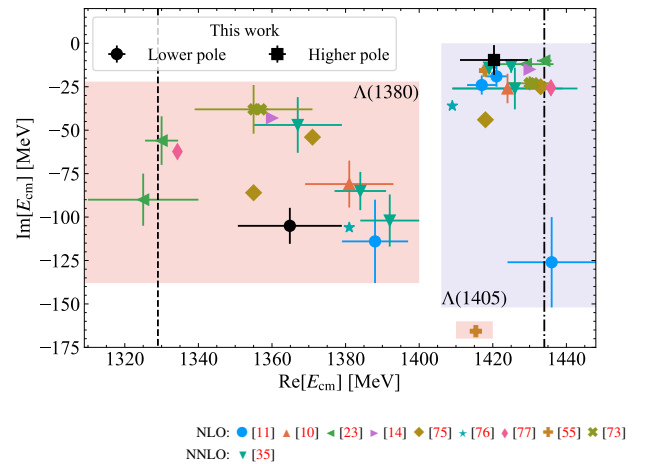


FIG. 3. Positions of the two  $\Lambda(1405)$  poles (color in black) up to NLO obtained in the present study in comparison with the results of other previous studies [10, 11, 14, 23, 35, 55, 73, 75–77].

Next, we show our prediction for the trajectories of the poles towards the SU(3) limit over the  $\text{Tr}[M] = C$  trajectory in Fig. 5, where we show the results at LO and up to NLO. We see that, at LO (LO+NLO), the lower pole evolves from a resonance into a virtual state at  $m_\pi = 198$  (173) MeV. Then, it becomes a bound state at  $m_\pi = 242$  (292) MeV and a singlet pole when it reaches the symmetric line. On the other hand, the higher pole changes from a resonance to a bound state at

<sup>3</sup> The pole positions are given in the irreducible representation basis. This basis and the particle basis are related through Clebsch-Gordan SU(3) coefficients [74].

$m_\pi = 417$  (371) MeV, close to the symmetric point. The higher pole of the  $\Lambda(1405)$  and the  $\Lambda(1680)$  belong to the octet representations 8 and 8', respectively, the same as in the leading order.

With this, we can also make a prediction for the evolution of the two poles over the  $m_s = m_{s,phy}$  trajectory towards the SU(3) symmetric line. This is shown in Fig. 6. In this case, we obtain that the symmetric point corresponds to  $m_\pi = 758$  MeV and  $m_B = 1592(78)(64)$  MeV. These values are also consistent with previous analysis of the baryon masses [59]. Since now the  $\bar{K}$  and the  $\Sigma$  masses increase with the pion mass, see Supplemental Material [67], we obtain that the real parts of the two poles, which couple significantly to  $\bar{K}N$  and  $\pi\Sigma$ , rise much faster than in the  $\text{Tr}[M] = C$  trajectory, reaching the values of the energies for the singlet and octet,  $E_s^{(1)} = 2268(16)$  MeV, and  $E_s^{(8)} = 2327(12)$  MeV, respectively, at the symmetric line. When the NLO is included, we obtain  $E_s^{(1)} = 2262(9)$  MeV,  $E_s^{(8)} = 2304(10)$  MeV, and  $E_s^{(8')} = 2356(42) - i0.6(6)$  MeV.

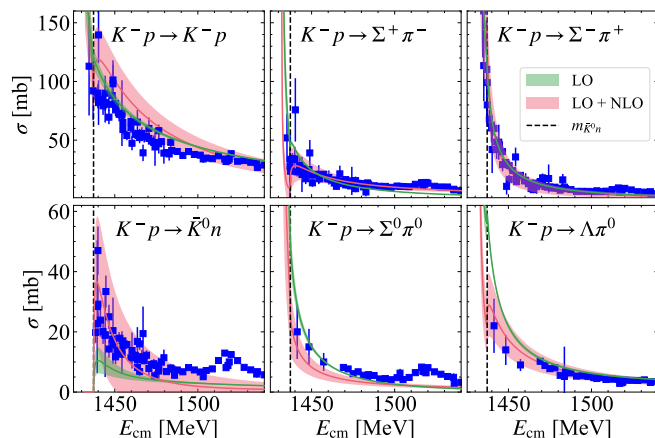


FIG. 4. Comparison of the predicted cross-sections and the experimental data. The error bands of the cross sections are constrained by the correlation matrix of the fit to the LQCD energy levels.

Finally, we compare with previous works. In [55], the energies of the two poles at the SU(3) symmetric point at LO become 1704 and 1788 MeV for the singlet and two octets, respectively. These values differ more than 150 MeV than the ones obtained here, while we obtain similar small breaking effect at NLO leading to two separated octets of 16 MeV. However, note that the pion mass used in [55] at the SU(3) symmetric point is 512 MeV. In addition, while in Ref. [55] is predicted that at NLO, the trajectories exchange with respect to the LO, the only significant difference between the LO and NLO results we get here is that the width of the lower pole is larger at NLO. This is consistent with the dominance of the LO contribution observed in previous works [3, 5, 35, 78]. We would like to stress that our analysis is based on the recent LQCD data on baryon masses, pseudoscalar meson masses, and decay constants along several chiral trajectories,  $\text{Tr}[M] = C$ ,  $m_s = m_{s,phy}$ , and  $m_{u(d)} = m_s$  for the CLS ensembles, while in Ref. [55], the  $b$ 's are fixed to old data from Ref. [49] for only one trajectory,  $m_s = m_{s,phy}$ , and similarly for the

meson parameters [79]. Moreover, the scheme used for the subtraction constant is also different. While the subtraction constants in Ref. [55] change with the scale  $\mu = m_{Bi}$  [80, 81], in this work we fix the scale  $\mu = 630$  MeV, and the subtraction constant quark mass dependence is obtained by comparing the loop functions obtained in the cutoff and DR schemes [70]. In addition, the values of the subtraction constants obtained in this work are close to the natural value,  $a \simeq -2$  [9]. Concretely, one gets from Eq. (4),  $a_{\pi\Sigma} = -2.30(-2.33)$ , and  $a_{\bar{K}N} = -2.10(-2.07)$  for  $m_\pi = 200$  MeV (138 MeV). The subtraction constant in the SU(3) limit is  $a_i = -2.24$ .

Indeed, the pole trajectories in the chiral unitary framework were studied first in [5, 82] at LO and in [78] up to NLO. The results of [5, 78, 82] show that these trajectories at LO and up to NLO are similar. Here, we are also consistent with the qualitative trends obtained in [5, 78, 82] where a simple quadratic formula for the meson and baryon masses is assumed<sup>4</sup>. However, the values obtained here for the poles at the symmetric point differ significantly from the ones in [5, 78, 82]. The reason is that we have used a more realistic description of the baryon masses based on the covariant chiral perturbation theory and recent LQCD data. Our work is the first one that shows agreement between both experimental and LQCD data consistently. As a result, we have made realistic predictions concerning the quark mass dependence of the two-poles of the  $\Lambda(1405)$ .

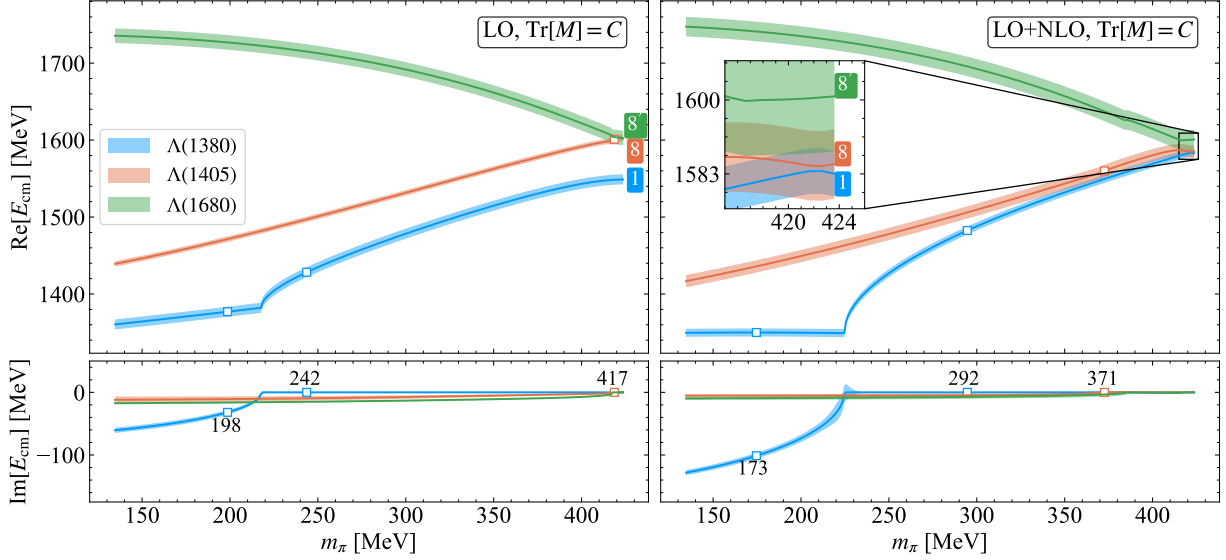
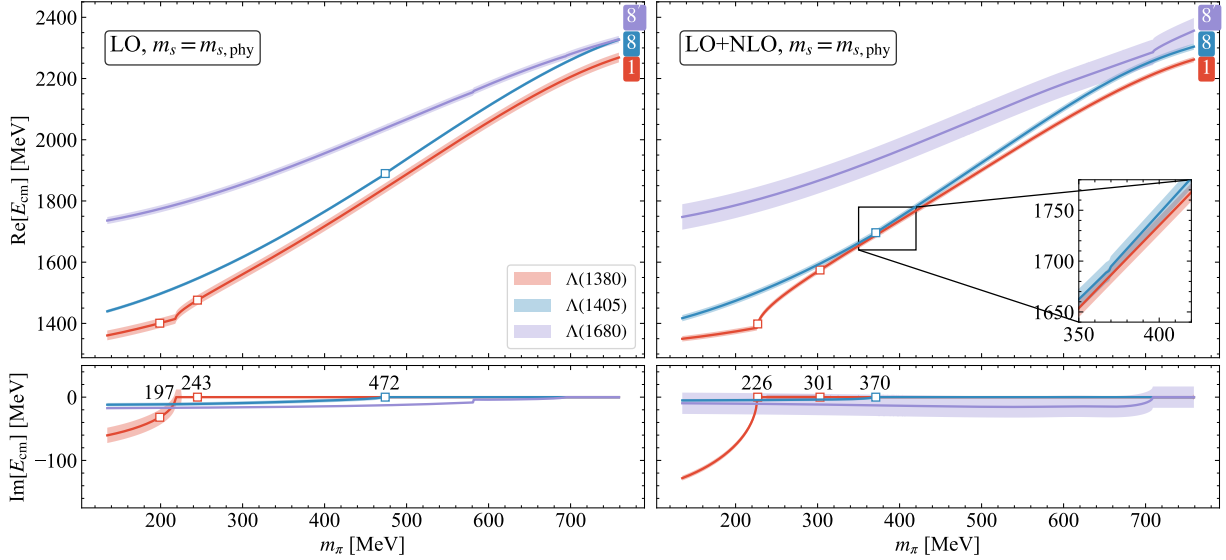
#### IV. CONCLUSION AND OUTLOOK

In this work, we have analyzed the LQCD data on  $\pi\Sigma - \bar{K}N$  scattering for  $I = 0$  (energy levels) and data on the quark mass dependence of the octet baryon masses. The theoretical framework is based on the NLO chiral Lagrangians for the meson-baryon interaction and covariant baryon chiral perturbation theory for the baryon masses. We have also implemented the quark mass dependence of the subtraction constants in the meson-baryon loops following the scheme of [70]. Our analysis took into account recent LQCD data on the baryon masses, meson masses, and pseudoscalar decay constants, and the quark mass dependence of the subtraction constant, which turns out to be of natural size. Thus, we have obtained the most precise determination of the trajectories of the two-pole  $\Lambda(1405)$  towards the symmetric line over the  $\text{Tr}[M] = C$  curve. The extrapolation of our results for the two-pole positions at  $m_\pi \simeq 200$  MeV to the physical point is consistent with the experiment. Remarkably, our results also agree with the cross-section data. Therefore, for the first time, consistency between the chiral unitary approach predictions for the two-pole structure, the recent LQCD scattering data [51, 52], and the experimental data, is shown. We found that both

<sup>4</sup> In [5, 78, 82], the authors take formulas of the type,  $m_i^2 = m_0^2 + x(m_i^2 - m_0^2)$ , and  $M_i(x) = M_0 + x(M_i - M_0)$ , where  $x = 0$  corresponds to the SU(3) symmetric point and  $x = 1$  to the physical point,  $m_i$  and  $M_i$  stand for the pseudoscalar meson and baryon masses in the physical point, and the subindex 0 refers to the symmetric point.

TABLE III. Pole positions of the  $\Lambda(1405)$  given as  $[M, \Gamma/2]$  for  $m_\pi = 138, 200,$  and  $423$  MeV.

$m_\pi$ [MeV]	138		200		423		
	$z_1$	$z_2$	$z_1$	$z_2$	$z_1$	$z_2$	$z_3$
Pole [MeV]	[1365(4)(10), 105(3)(7)]	[1420(4)(5), 10(3)(6)]	1380(7)(10)	[1454(5)(7), 13(4)(6)]	1583(5)(1)	1585(8)(2)	1601(12)(2)
$ g_{\pi\Sigma} $	2.8(1)(3)	1.0(2)(4)	3.8(9)(10)	1.3(2)(4)	0.9(4)(8)	1.4(4)(6)	1.4(3)(1)
$ g_{\bar{K}N} $	1.8(3)(6)	3.0(2)(4)	1.7(3)(3)	3.0(2)(4)	1.1(4)(6)	2.1(5)(2)	0.6(6)(2)
$\frac{ g_{\pi\Sigma} }{ g_{\bar{K}N} }$	1.6(9)(3)	0.3(1)(1)	2.4(8)(10)	0.4(1)(1)	0.8(5)(9)	0.7(5)(2)	2.3(10)(10)

FIG. 5. Trajectories of the three poles at LO (left panel) and up to NLO (right panel) for the  $\Lambda(1405)$  and  $\Lambda(1680)$ . The uncertainties of trajectories originate from the statistical errors and the lattice spacing error.FIG. 6. Trajectories of the three poles at LO (left panel) and up to NLO (right panel) for the  $\Lambda(1405)$  and  $\Lambda(1680)$ . The uncertainties of trajectories originate from the statistical errors.

poles lie on the physical Riemann sheet at the symmetric point over the  $\text{Tr}[M] = C$  trajectory. While the lower pole belongs to the singlet and is located at  $E^{(1)} = 1583(5)(1)$  MeV, the higher pole belongs to the octet representation and has a mass  $E^{(8)} = 1585(8)(2)$  MeV. We have also predicted the evolution of the poles over the  $m_s = m_{s,phy}$  curve. In this trajectory, the symmetric point is reached at a higher pion mass, providing the values for the singlet and octet,  $E_s^{(1)} = 2268(16)$  MeV, and  $E_s^{(8)} = 2327(12)$  MeV. Our results for these pole locations differ more than 100 MeV from previous estimations [5, 55, 78].

Since the pole trajectories of the scattering amplitude are intimately connected to the nature of dynamically generated resonances through chiral dynamics and the SU(3) breaking pattern, we believe that the results obtained here strongly support the two-pole structure of the  $\Lambda(1405)$  generated from the  $\pi\Sigma - \bar{K}N$  interaction. Thus, this work significantly advances the comprehension of this long-standing puzzle, which is also essential to understanding the interaction between nuclei and strange mesons relevant to nuclear physics and astrophysics. This study can be extended to other states, such as the controversial  $N^*(1535)$ . The present work can also be tested in future LQCD simulations and experimental measurements [83].

## ACKNOWLEDGMENTS

We are grateful to J. A. Oller, J. R. Pelaez, S. Cruz-Alzaga, and F. Gil-Dominguez for useful discussions. We acknowledge to J. Bulava and the BaSc Collaboration, and the RQCD Collaboration for making the data available to us. R. M. acknowledges support from the CIDEAGENT program with Ref. CIDEAGENT/2019/015 and the PROMETEU program with Ref. CIPROM/2023/59, of the Generalitat Valenciana, and also from the Spanish Ministerio de Economía y Competitividad and European Union (NextGenerationEU/PRTR) by the grant with Ref. CNS2022-13614. L. S. G. acknowledges support from the National Key R&D Program of China under Grant No. 2023YFA1606700. This work is also partly supported by the Spanish Ministerio de Economía y Competitividad (MINECO) and European FEDER funds under Contracts No. FIS2017-84038-C2-1-P B, PID2020-112777GB-I00, and by Generalitat Valenciana under contract PROMETEO/2020/023. This project has received funding from the European Union Horizon 2020 research and innovation program under the program H2020-INFRAIA-2018-1, grant agreement No. 824093 of the STRONG-2020 project.

- 
- [1] R. H. Dalitz and S. F. Tuan, *Phys. Rev. Lett.* **2**, 425 (1959).  
 [2] R. H. Dalitz and S. F. Tuan, *Annals Phys.* **10**, 307 (1960).  
 [3] E. Oset and A. Ramos, *Nucl. Phys. A* **635**, 99 (1998), arXiv:nucl-th/9711022.  
 [4] J. A. Oller and U. G. Meissner, *Phys. Lett. B* **500**, 263 (2001), arXiv:hep-ph/0011146.  
 [5] D. Jido, J. A. Oller, E. Oset, A. Ramos, and U. G. Meissner, *Nucl. Phys. A* **725**, 181 (2003), arXiv:nucl-th/0303062.  
 [6] B. Borasoy, R. Nissler, and W. Weise, *Eur. Phys. J. A* **25**, 79 (2005), arXiv:hep-ph/0505239.  
 [7] B. Borasoy, U. G. Meissner, and R. Nissler, *Phys. Rev. C* **74**, 055201 (2006), arXiv:hep-ph/0606108.  
 [8] T. Hyodo and W. Weise, *Phys. Rev. C* **77**, 035204 (2008), arXiv:0712.1613 [nucl-th].  
 [9] Y. Ikeda, T. Hyodo, and W. Weise, *Phys. Lett. B* **706**, 63 (2011), arXiv:1109.3005 [nucl-th].  
 [10] Y. Ikeda, T. Hyodo, and W. Weise, *Nucl. Phys. A* **881**, 98 (2012), arXiv:1201.6549 [nucl-th].  
 [11] Z.-H. Guo and J. A. Oller, *Phys. Rev. C* **87**, 035202 (2013), arXiv:1210.3485 [hep-ph].  
 [12] A. Feijoo, V. K. Magas, and A. Ramos, *Phys. Rev. C* **92**, 015206 (2015), arXiv:1502.07956 [nucl-th].  
 [13] A. Feijoo, V. Magas, and A. Ramos, *Phys. Rev. C* **99**, 035211 (2019), arXiv:1810.07600 [hep-ph].  
 [14] D. Sadasivan, M. Mai, and M. Döring, *Phys. Lett. B* **789**, 329 (2019), arXiv:1805.04534 [nucl-th].  
 [15] R. Molina, C.-W. Xiao, W.-H. Liang, and E. Oset, *Phys. Rev. D* **109**, 054002 (2024), arXiv:2310.12593 [hep-ph].  
 [16] P. A. Zyla *et al.* (Particle Data Group), *PTEP* **2020**, 083C01 (2020).  
 [17] K. Moriya *et al.* (CLAS), *Phys. Rev. Lett.* **112**, 082004 (2014), arXiv:1402.2296 [hep-ex].  
 [18] N. Kaiser, P. B. Siegel, and W. Weise, *Nucl. Phys. A* **594**, 325 (1995), arXiv:nucl-th/9505043.  
 [19] N. Kaiser, T. Waas, and W. Weise, *Nucl. Phys. A* **612**, 297 (1997), arXiv:hep-ph/9607459.  
 [20] J. Nieves and E. Ruiz Arriola, *Phys. Rev. D* **64**, 116008 (2001), arXiv:hep-ph/0104307.  
 [21] D. Jido, E. Oset, and A. Ramos, *Phys. Rev. C* **66**, 055203 (2002), arXiv:nucl-th/0208010.  
 [22] A. Cieplý and V. Křečřířik, *Nucl. Phys. A* **940**, 311 (2015), arXiv:1501.06415 [nucl-th].  
 [23] M. Mai and U.-G. Meißner, *Eur. Phys. J. A* **51**, 30 (2015), arXiv:1411.7884 [hep-ph].  
 [24] M. Mai and U.-G. Meissner, *Nucl. Phys. A* **900**, 51 (2013), arXiv:1202.2030 [nucl-th].  
 [25] A. Cieplý, M. Mai, U.-G. Meißner, and J. Smejkal, *Nucl. Phys. A* **954**, 17 (2016), arXiv:1603.02531 [hep-ph].  
 [26] J. Gasser, H. Leutwyler, and M. E. Sainio, *Phys. Lett. B* **253**, 252 (1991).  
 [27] M. Niiyama *et al.*, *Phys. Rev. C* **78**, 035202 (2008), arXiv:0805.4051 [hep-ex].  
 [28] K. Moriya *et al.* (CLAS), *Phys. Rev. C* **87**, 035206 (2013), arXiv:1301.5000 [nucl-ex].  
 [29] H. Y. Lu *et al.* (CLAS), *Phys. Rev. C* **88**, 045202 (2013), arXiv:1307.4411 [nucl-ex].  
 [30] I. Zychor *et al.*, *Phys. Lett. B* **660**, 167 (2008), arXiv:0705.1039 [nucl-ex].  
 [31] G. Agakishiev *et al.* (HADES), *Phys. Rev. C* **87**, 025201 (2013), arXiv:1208.0205 [nucl-ex].  
 [32] M. Hassanvand, S. Z. Kalantari, Y. Akaishi, and T. Yamazaki, *Phys. Rev. C* **87**, 055202 (2013), [Addendum: *Phys. Rev. C* **88**, 019905 (2013)], arXiv:1210.7725 [nucl-th].  
 [33] L. Roca and E. Oset, *Phys. Rev. C* **87**, 055201 (2013), arXiv:1301.5741 [nucl-th].  
 [34] M. Bayar, R. Pavao, S. Sakai, and E. Oset, *Phys. Rev. C* **97**, 035203 (2018), arXiv:1710.03964 [hep-ph].  
 [35] J.-X. Lu, L.-S. Geng, M. Doering, and M. Mai, *Phys. Rev. Lett.* **130**, 071902 (2023), arXiv:2209.02471 [hep-ph].  
 [36] M. Mai, *Eur. Phys. J. ST* **230**, 1593 (2021), arXiv:2010.00056

- [nucl-th].
- [37] U.-G. Meißner, *Symmetry* **12**, 981 (2020), [arXiv:2005.06909 \[hep-ph\]](#).
- [38] S. Acharya *et al.* (ALICE), *Phys. Rev. Lett.* **124**, 092301 (2020), [arXiv:1905.13470 \[nucl-ex\]](#).
- [39] S. Acharya *et al.* (ALICE), *Eur. Phys. J. C* **83**, 340 (2023), [arXiv:2205.15176 \[nucl-ex\]](#).
- [40] S. Aikawa *et al.* (J-PARC E31), *Phys. Lett. B* **837**, 137637 (2023), [arXiv:2209.08254 \[nucl-ex\]](#).
- [41] P. Gubler, T. T. Takahashi, and M. Oka, *Phys. Rev. D* **94**, 114518 (2016), [arXiv:1609.01889 \[hep-lat\]](#).
- [42] B. J. Menadue, W. Kamleh, D. B. Leinweber, and M. S. Mahbub, *Phys. Rev. Lett.* **108**, 112001 (2012), [arXiv:1109.6716 \[hep-lat\]](#).
- [43] G. P. Engel, C. B. Lang, and A. Schäfer (BGR (Bern-Graz-Regensburg)), *Phys. Rev. D* **87**, 034502 (2013), [arXiv:1212.2032 \[hep-lat\]](#).
- [44] G. P. Engel, C. B. Lang, D. Mohler, and A. Schäfer (BGR), *Phys. Rev. D* **87**, 074504 (2013), [arXiv:1301.4318 \[hep-lat\]](#).
- [45] Y. Nemoto, N. Nakajima, H. Matsufuru, and H. Suganuma, *Phys. Rev. D* **68**, 094505 (2003), [arXiv:hep-lat/0302013](#).
- [46] T. Burch, C. Gattlinger, L. Y. Glozman, C. Hagen, D. Hierl, C. B. Lang, and A. Schafer, *Phys. Rev. D* **74**, 014504 (2006), [arXiv:hep-lat/0604019](#).
- [47] T. T. Takahashi and M. Oka, *Phys. Rev. D* **81**, 034505 (2010), [arXiv:0910.0686 \[hep-lat\]](#).
- [48] S. Meinel and G. Rendon, *Phys. Rev. D* **105**, L051505 (2022), [arXiv:2107.13084 \[hep-ph\]](#).
- [49] J. M. M. Hall, W. Kamleh, D. B. Leinweber, B. J. Menadue, B. J. Owen, A. W. Thomas, and R. D. Young, *Phys. Rev. Lett.* **114**, 132002 (2015), [arXiv:1411.3402 \[hep-lat\]](#).
- [50] A. Martinez Torres, M. Bayar, D. Jido, and E. Oset, *Phys. Rev. C* **86**, 055201 (2012), [arXiv:1202.4297 \[hep-lat\]](#).
- [51] J. Bulava *et al.* (Baryon Scattering (BaSc)), *Phys. Rev. D* **109**, 014511 (2024), [arXiv:2307.13471 \[hep-lat\]](#).
- [52] J. Bulava *et al.* (Baryon Scattering (BaSc)), *Phys. Rev. Lett.* **132**, 051901 (2024), [arXiv:2307.10413 \[hep-lat\]](#).
- [53] R. Molina and M. Döring, *Phys. Rev. D* **94**, 056010 (2016), [Addendum: *Phys.Rev.D* 94, 079901 (2016)], [arXiv:1512.05831 \[hep-lat\]](#).
- [54] R. Pavao, P. Gubler, P. Fernandez-Soler, J. Nieves, M. Oka, and T. T. Takahashi, *Phys. Lett. B* **820**, 136473 (2021), [arXiv:2010.01270 \[hep-lat\]](#).
- [55] F.-K. Guo, Y. Kamiya, M. Mai, and U.-G. Meißner, *Phys. Lett. B* **846**, 138264 (2023), [arXiv:2308.07658 \[hep-ph\]](#).
- [56] J.-M. Xie, J.-X. Lu, L.-S. Geng, and B.-S. Zou, *Phys. Rev. D* **108**, L111502 (2023), [arXiv:2307.11631 \[hep-ph\]](#).
- [57] X.-L. Ren, (2024), [arXiv:2404.02720 \[hep-ph\]](#).
- [58] S. Aoki *et al.* (PACS-CS), *Phys. Rev. D* **79**, 034503 (2009), [arXiv:0807.1661 \[hep-lat\]](#).
- [59] X. L. Ren, L. S. Geng, J. Martin Camalich, J. Meng, and H. Toki, *JHEP* **12**, 073 (2012), [arXiv:1209.3641 \[nucl-th\]](#).
- [60] G. S. Bali, S. Collins, P. Georg, D. Jenkins, P. Korcyl, A. Schäfer, E. E. Scholz, J. Simeth, W. Söldner, and S. Weishäupl (RQCD), *JHEP* **05**, 035 (2023), [arXiv:2211.03744 \[hep-lat\]](#).
- [61] A. Pich, *Rept. Prog. Phys.* **58**, 563 (1995), [arXiv:hep-ph/9502366](#).
- [62] G. Ecker, *Prog. Part. Nucl. Phys.* **35**, 1 (1995), [arXiv:hep-ph/9501357](#).
- [63] V. Bernard, N. Kaiser, and U.-G. Meissner, *Int. J. Mod. Phys. E* **4**, 193 (1995), [arXiv:hep-ph/9501384](#).
- [64] U. G. Meissner, *Rept. Prog. Phys.* **56**, 903 (1993), [arXiv:hep-ph/9302247](#).
- [65] M. Frink and U.-G. Meissner, *Eur. Phys. J. A* **29**, 255 (2006), [arXiv:hep-ph/0609256](#).
- [66] J. A. Oller, M. Verbeni, and J. Prades, *JHEP* **09**, 079 (2006), [arXiv:hep-ph/0608204](#).
- [67] See Supplemental Material at [URL\\_will\\_be\\_inserted\\_by\\_publisher](#), for additional discussions about the method and results.
- [68] R. Molina and J. Ruiz de Elvira, *JHEP* **11**, 017 (2020), [arXiv:2005.13584 \[hep-lat\]](#).
- [69] J. A. Oller, E. Oset, and J. R. Pelaez, *Phys. Rev. D* **59**, 074001 (1999), [Erratum: *Phys.Rev.D* 60, 099906 (1999), Erratum: *Phys.Rev.D* 75, 099903 (2007)], [arXiv:hep-ph/9804209](#).
- [70] J. A. Oller, *Prog. Part. Nucl. Phys.* **110**, 103728 (2020), [arXiv:1909.00370 \[hep-ph\]](#).
- [71] A. Martinez Torres, L. R. Dai, C. Koren, D. Jido, and E. Oset, *Phys. Rev. D* **85**, 014027 (2012), [arXiv:1109.0396 \[hep-lat\]](#).
- [72] M. Doring, U. G. Meissner, E. Oset, and A. Rusetsky, *Eur. Phys. J. A* **48**, 114 (2012), [arXiv:1205.4838 \[hep-lat\]](#).
- [73] D. Sadasivan, M. Mai, M. Döring, U.-G. Meißner, F. Amorim, J. P. Klucik, J.-X. Lu, and L.-S. Geng, *Front. Phys.* **11**, 1139236 (2023), [arXiv:2212.10415 \[nucl-th\]](#).
- [74] J. J. de Swart, in *The Eightfold Way* (CRC Press, 2018) pp. 120–143.
- [75] A. Cieply and J. Smejkal, *Nucl. Phys. A* **881**, 115 (2012), [arXiv:1112.0917 \[nucl-th\]](#).
- [76] N. V. Shevchenko, *Phys. Rev. C* **85**, 034001 (2012), [arXiv:1103.4974 \[nucl-th\]](#).
- [77] J. Haidenbauer, G. Krein, U.-G. Meissner, and L. Tolos, *Eur. Phys. J. A* **47**, 18 (2011), [arXiv:1008.3794 \[nucl-th\]](#).
- [78] P. C. Bruns and A. Cieplý, *Nucl. Phys. A* **1019**, 122378 (2022), [arXiv:2109.03109 \[hep-ph\]](#).
- [79] J. Nebreda and J. R. Pelaez., *Phys. Rev. D* **81**, 054035 (2010), [arXiv:1001.5237 \[hep-ph\]](#).
- [80] M. F. M. Lutz and E. E. Kolomeitsev, *Nucl. Phys. A* **700**, 193 (2002), [arXiv:nucl-th/0105042](#).
- [81] T. Hyodo, D. Jido, and A. Hosaka, *Phys. Rev. C* **78**, 025203 (2008), [arXiv:0803.2550 \[nucl-th\]](#).
- [82] C. Garcia-Recio, M. F. M. Lutz, and J. Nieves, *Phys. Lett. B* **582**, 49 (2004), [arXiv:nucl-th/0305100](#).
- [83] Y.-B. He, X.-H. Liu, L.-S. Geng, F.-K. Guo, and J.-J. Xie, (2024), [arXiv:2407.13486 \[hep-ph\]](#).
- [84] J. Gasser and H. Leutwyler, *Nucl. Phys. B* **250**, 465 (1985).
- [85] J. Martin Camalich, L. S. Geng, and M. J. Vicente Vacas, *Phys. Rev. D* **82**, 074504 (2010), [arXiv:1003.1929 \[hep-lat\]](#).
- [86] B. Borasoy, *Phys. Rev. D* **59**, 054021 (1999), [arXiv:hep-ph/9811411](#).



## SUPPLEMENTAL MATERIAL

This supplemental material presents details regarding the fitting results and several intermediate results necessary to obtain the primary results, namely the inelasticities and phase shifts, the correlation matrix of the fit to the energy levels, the fit to the octet baryon masses, the fitting results at LO, and an alternative representation of the poles' trajectories.

### A. Phase shifts and inelasticities

Inelasticities  $\eta$  and phase shifts  $\delta_{\pi\Sigma}$  and  $\delta_{\bar{K}N}$  up to NLO as a function of the center-of-mass energy difference with respect to the  $\pi\Sigma$  threshold is given in Fig. 7. Indeed, these agree very well with the findings in the LQCD simulation [51, 52].

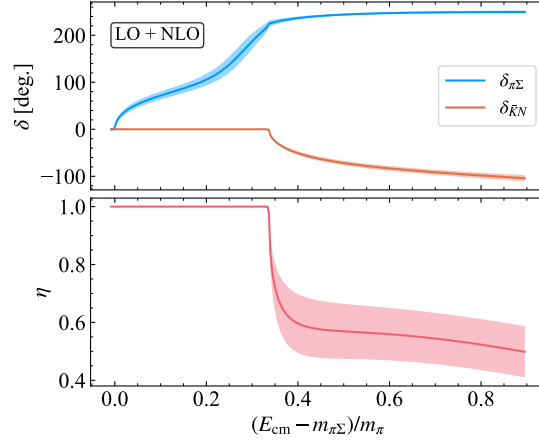


FIG. 7. Inelasticities  $\eta$  and phase shifts  $\delta_{\pi\Sigma}$  and  $\delta_{\bar{K}N}$  up to NLO as a function of the center-of-mass energy difference with respect to the  $\pi\Sigma$  threshold.

### B. The correlation matrix of the fit to the energy levels

The heat map of the correlation matrix between the LECs is given in Fig. 8.

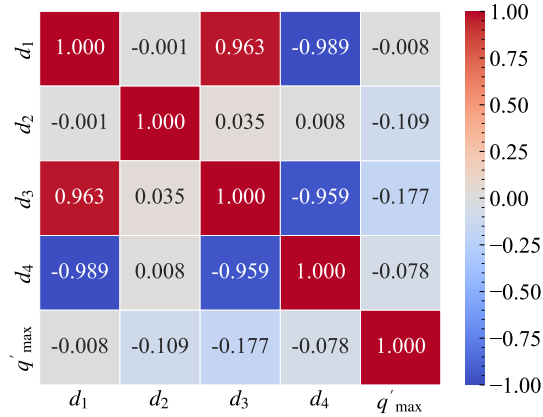


FIG. 8. Heat map of the correlation matrix for the LECs from the fit to the energy levels.

We observe that the LECs  $d_1, d_3, d_4$  are very much correlated. However, they are not much related to the  $q'_{\max}$  parameter.

### C. Meson masses

The pseudoscalar meson masses up to NLO in ChPT are given by [84]

$$m_\pi^2 = M_{0\pi}^2 \left[ 1 + \mu_\pi - \frac{\mu_\eta}{3} + \frac{16M_{0K}^2}{f_0^2} (2L_6^r - L_4^r) \right] + \frac{8M_{0\pi}^2}{f_0^2} (2L_6^r + 2L_8^r - L_4^r - L_5^r), \quad (14)$$

$$m_K^2 = M_{0K}^2 \left[ 1 + \frac{2\mu_\eta}{3} + \frac{8M_{0\pi}^2}{f_0^2} (2L_6^r - L_4^r) + \frac{8M_{0K}^2}{f_0^2} (4L_6^r + 2L_8^r - 2L_4^r - L_5^r) \right], \quad (15)$$

$$m_\eta^2 = M_{0\eta}^2 \left[ 1 + 2\mu_K - \frac{4}{3}\mu_\eta + \frac{8M_{0\eta}^2}{f_0^2} (2L_8^r - L_5^r) + \frac{8}{f_0^2} (2M_{0K}^2 + M_{0\pi}^2) (2L_6^r - L_4^r) \right] \\ + M_{0\pi}^2 \left[ -\mu_\pi + \frac{2}{3}\mu_K + \frac{1}{3}\mu_\eta \right] + \frac{128}{9f_0^2} (M_{0K}^2 - M_{0\pi}^2)^2 (3L_7 + L_8^r), \quad (16)$$

with

$$\mu_P = \frac{M_{0P}^2}{32\pi^2 f_0^2} \log \frac{M_{0P}^2}{\mu_r^2}, \quad P = \pi, K, \eta. \quad (17)$$

The superscript  $r$  denotes renormalized LECs, which carry the dependence on the regularization scale  $\mu_r$  [84]. In the above equation,  $M_{0P}$ , with  $P = \pi, K, \eta$ , represent the pseudoscalar meson masses at LO and  $f_0$  the decay constant in the chiral limit. Here, we take  $\mu_r = 770$  MeV and  $f_0 = 80$  MeV as in Ref. [68]. The LECs  $L_i$  are taken from Table X of [68].

### D. Baryon masses

We analyze the data from Ref. [60] for the baryon masses of the CLS ensembles using the one-loop NLO covariant baryon chiral perturbation theory [85].

$$m_B = m_0 + m_B^{(2)} + m_B^{(3)}, \quad (18)$$

where

$$m_B^{(2)} = \sum_{\phi=\pi,K} -\xi_{B,\phi}^{(a)} m_\phi^2, \quad (19)$$

and

$$m_B^{(3)} = \sum_{\phi=\pi,K,\eta} \frac{1}{(4\pi f_\phi)^2} \xi_{B,\phi}^{(b)} H_B^{(b)}(m_\phi), \quad (20)$$

where  $m_0$  stands for the baryon mass in the chiral limit, and  $m_B^{(2)}$  and  $m_B^{(3)}$  represent the polynomial and one-loop contributions, respectively. The coefficients  $\xi_{B,\phi}^{(a)}$  and  $\xi_{B,\phi}^{(b)}$  can be found in Ref. [85]. These are combinations of the pertinent LECs,  $b_0, b_D, b_F, D, F$ . The EOMS loop-function  $H_B^{(b)}(m_\phi)$  can be found in Ref. [60]. The baryon axial coupling constants  $D$  and  $F$  are fixed to be [86],

$$D = 0.80, \quad F = 0.46. \quad (21)$$

In Ref. [60] there are three types of chiral trajectories, i.e.,  $\text{Tr}[M] = C$ ,  $m_s = m_{s,\text{phy}}$ , and  $m_s = m_l$ , where  $l = u, d$ . In Eqs. (14)-(15), the pseudoscalar mesons' masses depend on  $m_{0\pi}$  and  $m_{0K}$ . The Gell-Mann-Okubo relation gives

$$m_{0K}^2 = B_0 C - \frac{m_{0\pi}^2}{2}, \quad m_{0K}^2 = B_0 m_{s,\text{phy}} + \frac{m_{0\pi}^2}{2} \quad (22)$$

with respect to  $\text{Tr}[M] = C$  and  $m_s = m_{s,\text{phy}}$ , respectively. The free parameters needed to fit the hadron masses in Ref. [60] are  $B_0C$ ,  $B_0m_s$ ,  $m_0$ ,  $b_0$ ,  $b_D$ , and  $b_F$ . The results of the fits are plotted in Fig. 9. In Ref. [60], the authors have corrected the systematic effects, e.g., the finite volume and finite lattice spacing. The details are explained in Sec. 4.2 of Ref. [60]. We have taken the data from Ref. [60] already corrected for the systematic effects, and these are the data that we have used. The covariance matrix for the octet baryon masses and the pseudo-scalar meson masses is also included in this fit. Indeed, in Ref. [60], the authors also perform a fit of the baryon masses using the Baryon Chiral Perturbation theory up to  $\mathcal{O}(p^3)$ . The reason why the LECs from Ref. [60] are not used here is because the parameters  $D$  and  $F$  in Eq. (18) of Ref. [60] are also fitted to the data. However, the constants  $D$  and  $F$  should be determined by fitting to the semi-leptonic decays  $B \rightarrow B' + e^- + \bar{\nu}_e$  at tree level [86]. For this reason, we have fixed  $D$  and  $F$  to the values given in Ref. [86]. The values that we obtain from the fit are given in Table IV, where we also show the LECs obtained in Ref. [60] for comparison. The correlations between the parameters are given in Fig. 10. In particular, we observe a very high correlation between the  $m_0$  and  $b_0$  parameters. It can be seen that the LECs obtained here are compatible within uncertainties with the ones given in [60].

TABLE IV. Free parameters fixed by the hadron masses in Ref. [60]. The first uncertainty is statistical, and the second comes from the uncertainty in the lattice spacing [60]. Our results are compared with those obtained in Ref. [60].

	$\sqrt{B_0C}$ [MeV]	$\sqrt{B_0m_{s,\text{phy}}}$ [MeV]	$m_0$ [MeV]	$b_0$ [GeV $^{-1}$ ]	$b_D$ [GeV $^{-1}$ ]	$b_F$ [GeV $^{-1}$ ]
This work	488(38)(42)	474(50)(55)	805(40)(40)	-0.665(40)(28)	0.062(26)(8)	-0.354(18)(9)
BChPT FV [60]	...	...	821 $^{(71)}$ (53)	-0.739 $^{(70)}$ (84)	0.056 $^{(43)}$ (39)	-0.44 $^{(40)}$ (26)

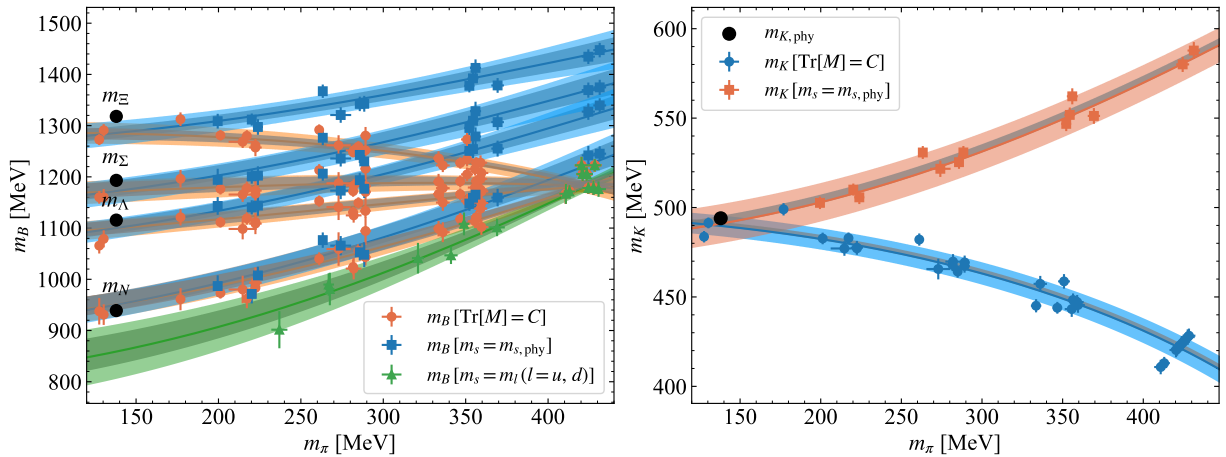


FIG. 9. Fits to the hadron masses. The data are provided by RQCD [60]. The circles, squares, and triangles denote the  $\text{Tr}[M] = C$ ,  $m_s = m_{s,\text{phy}}$  trajectories, and the symmetric line  $m_s = m_l$ , where  $l = u, d$ , respectively. The circles in black are the physical masses of the hadrons. The colored error bands consider the systematic and statistical errors of the hadron masses. The error bands in gray are the results where only the statistical errors are considered.

### E. Results for the LO fit

At LO, we have only one free parameter, i.e., the cutoff  $q'_{\text{max}}$ . We follow the scheme of [70] for  $a(\mu)$ . The reduced- $\chi^2$  obtained is  $\chi^2/\text{dof} = 3.2$ . The cutoff value obtained is

$$q'_{\text{max}} = 632 \pm 90 \text{ MeV}. \quad (23)$$

The pole positions of the  $\Lambda(1405)$  for  $m_\pi = 138, 200$ , and  $423$  MeV are given in Table V. At the physical point, they are close to the ones at NLO. For  $m_\pi \simeq 200$  MeV, the lower pole is a bound state instead of a resonance or a virtual state, whereas the higher pole is still a resonance with a mass close to the NLO result.

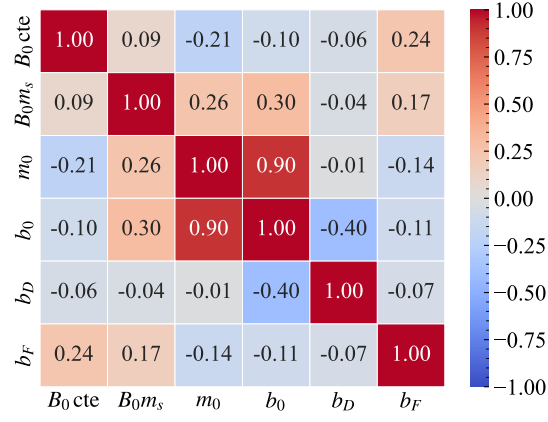


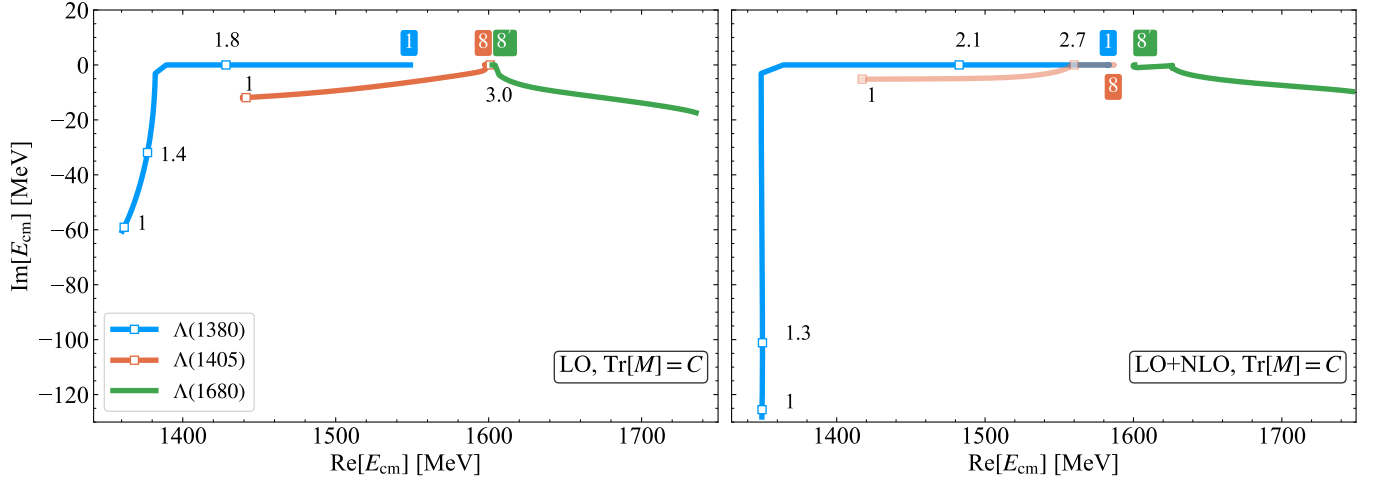
FIG. 10. Correlations between the parameters obtained from the fit to the octet baryon masses.

TABLE V. Pole positions of the  $\Lambda(1405)$  at LO with the cutoff  $q'_{\text{max}}$  fixed by energy levels. In this fit, the lower pole becomes a bound state instead of a resonance. The higher pole is a resonance.

$m_\pi$ [MeV]	138		200		423	
	$z_1$	$z_2$	$z_1$	$z_2$	$z_1$	$z_2$
Pole [MeV]	[1364(8), 38(11)]	[1439(1), 18(5)]	1397(3)	[1472(1), 12(2)]	1549(7)	1602(4)
$ g_{\pi\Sigma} $	2.4(2)	1.6(1)	0.7(3)	1.3(0.2)	3.5(1)	0.1(7)
$ g_{\bar{K}N} $	2.2(2)	2.4(1)	0.7(4)	2.1(0.03)	2.3(1)	0.3(2)
$\frac{ g_{\pi\Sigma} }{ g_{\bar{K}N} }$	1.1(2)	0.7(1)	1.0(1)	0.7(1)	1.5(1)	0.2(9)

### F. Pole trajectories from the SU(3) limit to the physical values

In this section, we provide an alternative way to represent the trajectories of the three poles at LO and up to NLO. The results are shown in Fig. 11. As one can see from this figure, the trajectories are qualitatively similar, except that up to NLO, the lower pole becomes broader.

FIG. 11. Pole trajectories from the SU(3) limit, where  $r = m_\pi/m_{\pi,\text{phy}} = 3.07$ , to the physical value, with  $r = 1$ . The numbers in the figures are the values of the ratio  $r$ .

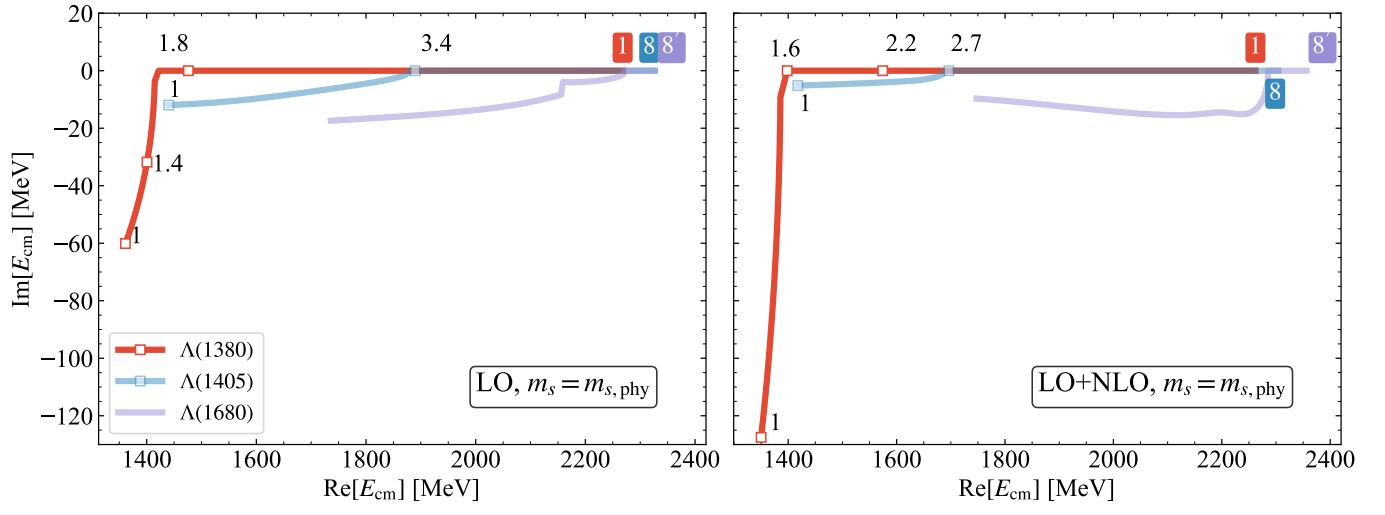


FIG. 12. Pole trajectories with  $m_s = m_{s,\text{phy}}$ .